RSC Advances

PAPER

View Article Online
View Journal | View Issue

Cite this: *RSC Adv.*, 2021, **11**, 32884

Functionalized poly(lactic acid) based nano-fabric for anti-viral applications†

Doli Hazarika, Naba Kumar Kalita, Amit Kumar and Vimal Katiyar *

Received 12th July 2021
Accepted 23rd August 2021

DOI: 10.1039/d1ra05352c

rsc.li/rsc-advances

This study endeavoured to explore and fabricate antiviral and antibacterial facemasks using zinc (oligo-lactate) (ZL), developed through a microwave synthesis technique. The prepared nano-fabric layer has excellent antiviral and antibacterial properties against Newcastle Disease Virus (NDV) and *E. coli* and *S. aureus*, respectively. Thermogravimetric analysis (TGA) of ZL shows a two-step thermal degradation, which confirms the formation of low molecular weight end group lactyl units with zinc ions. Another investigation using varying ZL concentration and silk nanocrystal (SNC) with poly(lactic acid) (PLA) and electrospinning them into nanofibres led to the fabrication of a facile and sustainable nanofabric that can be utilized as a protective layer for facemasks. Morphological analysis revealed the successful preparation of the nanofabric with proper distribution and uniformity in fibre diameter. Hydrophobicity of the prepared nanofabric confirmed excellent protection from water droplets that may transpire during coughing or sneezing by an infected individual. Breathability and reusability tests confirmed that the prepared facemask could be reused by ethanol washing without compromising its surface properties till 4 cycles. The PLA/ZL nanofabric layer demonstrated 97% antiviral efficacy against NDV in 10 minutes. In conclusion, the electrospun nanofabric layer can be used as a facemask having high hydrophobicity, good breathability, antibacterial, and antiviral properties to control the spread of contagious diseases.

Introduction

The aggressive necessity and application of facemasks and personal protective equipment (PPE) is now a new normal commodity. World Health Organization (WHO) has dictated standard safety procedures to make them wearable for every human being that may diminish the on-going infection risks of novel coronavirus (COVID-19). Facemasks with and without filters have been mostly used. Most commonly used facemasks are the surgical facemasks and respirator masks like P2 and N95. Moreover, the demand and supply of conventional polymers will give rise to new polluted episodes in near future.[1,2] For facemasks, in addition to filtering capacity, other factors are also important, such as user comfort and breathability. For instance, although the tight-fitted N95 respirators without any functional features are having superior filter capacity than the surgical masks but it lowers the breathability and sweating, causing discomfort after wearing for hours and most of them are prepared from conventional plastics.[3] However, utilization of sustainable and biodegradable based protective mask can lead us to overcome such problems of plastic pollution.[4] Most of the single-time usable masks are made of polypropylene, polyethylene, polyester, polyurethane, polyacrylonitrile, polystyrene, or polycarbonate.[5] The mask mainly consists of an inner layer as soft fibres, middle layer by melt-blown filter, and outer layer made with nonwoven fibres, having water-resistance. In general, fibrous materials were used to create particulate matter filters (PM), according to PM particulate size. PM is classified by PM 0.1 as ultrafine (<0.1 μm), PM 2.5, fine (0.1–2.5 μm size), and PM 10, course (2.5–10 μm).[6,7] For particles between the micro and nano range (~300 nm) electrospun nanofibres are proven to be more efficient that addresses two competing demands *i.e.* air filterability and air breathability. Focussing on nanoscale sized viruses, non-woven filters are better when compared to natural fibre cotton, petroleum-based polyester polymers, and some woven filters of advanced nature.[8] These nonwoven filters are made using electrospinning technique, a very efficient, low-cost technique to produce nanofibre mats, which are useful for several applications with distinct features including higher surface area to functionalize for uniform morphology, structural consistency properties, and desired properties.[9]

Disinfection of masks is another parameter that needs to be addressed. Therefore, masks with antiviral and antimicrobial activities can automatically kill contaminations during their service life. Hydrophilic or hydrophobic nature of the filter surface also plays an important role in providing favourable or unfavourable environments to different types of bacteria and viruses.[10]

Chemical Engineering Department, Indian Institute of Technology Guwahati, Assam-781039, India. E-mail: vkatiyar@iitg.ac.in

† Electronic supplementary information (ESI) available. See DOI: 10.1039/d1ra05352c

Zinc is a metal that has been purported to have antimicrobial properties. Zinc lactate is a salt obtained from reacted zinc and lactic acid (by bacterial fermentation). Various mechanisms have been reported that show antimicrobial properties of lactic acid and their salts as in an acidic environment, where they act as ionophores and decreases the intracellular pH in bacteria.[11–13] Zn lactate may possess protective effect and adjuvant therapy of COVID-19 infection for the whole world. From reports, zinc is considered as a potential supportive treatment in therapy of COVID-19 infection due to its antiviral effect and immune modulatory effect.[14] Silk is harvested from silkworms made by silk moth caterpillars, like (domesticated silk moth namely Eri, Muga, Tassar silk), *Bombyx mori*, and Robin moth, and *Hyalophora cecropia*. This silk fibre produced from their cocoons has been historically acting as "queen of textile'. Silk generally contains natural antimicrobial, antibacterial properties, which traits their potentiality to ward off the microbes, bacteria, and viruses.[15] Due to good biocompatibility, controllable biodegradability, and easy fabrication into different forms, such as fibres, films, gels, and three-dimensional scaffolds, silk fibroin has been used in biomedical materials for a long time.[16] Silk, due to its hydrophobic ends, have been extensively reported for its use as fabric and as protective respirators. A study has been performed on crystallinity and hydrophobicity improvement by tuning molecular structure into nano-level through various routes like alkali treatment, enzymatic hydrolysis, and partial acid-hydrolysis.[17]

Among different fabrication techniques, electrospinning technique is basically for nanofibre preparation, acting as a best replacement for microfibres and thin films. Thus, nanofibre filters can be gradually utilized for mask applications globally. Collectors used during electrospinning of fibres may consist of several materials. Nanofibres produced during this technique are collected in different collectors. Most commonly used collectors are aluminium foils while others are conductive cloth/paper, rotating wheel or rod, parallel bar, wire mesh *etc.*[18,19]

Among the various biodegradable polymers,[20] PLA has its applications in many manufacturing industries, such as in fibres, textiles, plasticulture, packaging industries, and service ware.[21,22] Furthermore, PLA exhibits excellent properties, such as nontoxicity, strong mechanical strength, and good fibre-forming ability. This made PLA a strong candidate for fabrication of nanofabrics.

It is reported that Zn powder, a cheap and easily available catalyst with microwave technique, was used to produce moderate molecular weight PLA with high purity.[23] Another study was reported on PLA and lactic acid-grafted-gum arabic by polycondensation reaction in a microwave reactor without using any catalyst, which was further solution casted with PLA for packaging applications.[24] Studies demonstrated the preparation of antimicrobial hybrid materials using PLA as nonwoven fabrics, where phosphoro-organic compound-fosfomycin was used as a coating and modifying agent. Nonwoven mats made of PLA/chitosan (PLA/CS) blend and PLA/CS blend contain silver (Ag) nanoparticles (Ag/PLA/CS) by electrospinning technique. The Ag blended nanocomposite had better antibacterial activity against the *E. coli* and *S. aureus* bacteria.[25] Another study was performed using electrospinning to prepare PLA/TiO_2 nanofibres, where it was found that the antibacterial activity improved under UV-A irradiation, and 0.75 wt% TiO_2 content nanofibres and films exhibited inhibition zones for *E. coli*, 4.86 $\pm$ 0.50 and 3.69 $\pm$ 0.40 mm and for *S. aureus*, 4.63 $\pm$ 0.45 and 5.98 $\pm$ 0.77 mm.[26] Another study prepared activated charcoal (A.C.) reinforced poly(lactic acid) (PLA) nanofibre membranes produced by electrospinning technique. It was found that Bacterial Filtration Efficiency (BFE) (% and Submicron Particle Filtration Efficiency) (%) is $\geq$98%, which meets the criterion as a personal protective equipment.[27]

This work focuses on easily available materials that would be beneficial for making face coverings, according to the guidelines of current public health, so that it can be worn during shortage of standard PPE. Currently, various studies have been associated with different materials, from natural fibre spinning to synthetic fabrics for preparing and making them commercially available. Even to block droplets and micro/nanoparticles, as well as identifying perfect facilitates for comfort, wearability, and reusability, face coverings are now gaining full attention to get relief from such situations. Therefore, in our current study, we have conducted an efficient strategy to prepare a material zinc oligo-lactate by microwave synthesis to act as a warrior during this pandemic situation. The prepared material with silk nanocrystal has been spun with compostable PLA into a nanofabric form for constructing face coverings. The novelty of the present work lies in the utilization of natural materials such as silk nanocrystals obtained from muga-silk waste. Its hydrophobic nature acts as a preventer for penetration and absorption of droplets, whereas ZL acts as an antiviral agent to prevent transmission of virus. In addition, the prepared fabric was tested for cleaning by its reusability test and porosity.

Materials and methods

Materials

Lactic acid, procured from Corbion, PURAC®, PLA grade 2003D, number-average molecular weight (Mn) of ~137 000 Da and weight-average (M_w) of ~200 000 Da) was supplied by Nature works, U.S.A. Chloroform (analytical grade, procured from Spectrochem, HPLC grade), *N*,*N*-dimethyl formamide (EMPLURA®). Acetic acid glacial (HIMEDIA), zinc powder pure (Merk), polypropylene (PP) nonwoven fabric (50 GSM SSMMS (spunbond $\times$ 2, meltblown $\times$ 2 and spunbond $\times$ 1) hydrophobic, supplied by KTEX NONWOVENS (taken for comparison).

Experimental sections

Preparation of SNC by acid hydrolysis treatment

For preparation of SNC, the steps followed are as reported herewith. Firstly, degumming and then using mechanical stirring by acid hydrolysis method, SNC was prepared.[17]

Synthesis of zinc oligo-lactate by microwave heating

Firstly, lactic acid was mixed with zinc powder in the ratio of 1 : 10 (molar ratio) with proper mixing in a round-bottom flask

(RBF) with a glass rod. The prepared mixture was placed inside a microwave and purged using N_2 atmosphere. Then, one neck was connected with a condenser, which is again connected to an RBF dipped in an ice bath to collect the condensed liquid. Microwave heating supports higher reaction rate and high product yield. Condensation polymerization reaction takes place during the preparation of ZL in a microwave at 140 °C, 1 h at 240 W, power under mode of "convection cum microwave". A heating belt (~100 °C), was connected over the pipe between the RBF and condenser. This usually avoids any unbound water condensation and any by products during reaction under an inert atmosphere. After completion of the reaction, solid mass (pH = 3.35) was taken out. The condensed unbound water was collected and measured. For the purpose of purification, the ZL was stirred in DI water for 1 h at room temperature to remove any unwanted lactic acid present. The white precipitate was centrifuged at 5000 rpm for 5 min, and then dried in the oven at 60 °C overnight and ground to powder. This powder was dispersed in water and was found to form a white precipitate with water at room temperature.

Reaction mechanism

Microwave assisted single pot polymerization route is favourable than the polycondensation and ring opening polymerization to synthesise a low molecular weight polymer. Microwave synthesis is environment friendly, less toxic in terms of performing at high temperature and for long time, no use of toxic catalyst and initiator. Initially, the reaction takes place between lactic acid (water-soluble) and Zn powder (insoluble in water) and the system water absorbs microwave energy and dielectric heating generates ion radicals. These ion radicals then react with water and form free hydroxyl radicals. The free radicals of lactic acid then attach together with the electropositive ions Zn^{2+} to functional groups *i.e.* OH form OLLA chain.

Preparation of nanocomposite solutions using electrospinning method

The electrospinning technique was used to prepare nonwoven nanofabric samples of PLA, PLA/ZL, and PLA/ZL/SNC over an aluminium substrate. Separately, 10 (w/v)% PLA solution was prepared by dissolving PLA in a chloroform : DMF (70 : 30) solvent mixture in a conical flask. Accordingly, the desired parameters are shown in Table 1. The same optimized parameters were used for the preparation of a nano-fibrous mat for inhibiting any role of process parameters and highlighting the effects of filler proportions in fibre morphology.

Characterization techniques

Nuclear magnetic resonance (NMR)

The structural linkage of the prepared ZL in macromolecular level was studied by dissolving it in deuterated water (D_2O) taking a concentration of 20 mg in 1 mL D_2O and vortex at lower speed. The proton ^1H NMR spectra for the prepared material was recorded by Bruker NMR spectrometer 600 MHz with 500 scans at room temperature with spectral range 0–10 ppm after filtering with PTFE 0.25 μm syringe filter for performing the analysis.

Fourier transform infrared spectrometry (FTIR)

The spectroscopic method for chemical structure analysis was done using infrared spectroscopy by FTIR. Make: PerkinElmer, S Model: Spectrum two. For both the powder and film sample, analysis was performed under attenuated total internal reflection mode (ATR) of range 450–4000 cm^{-1} with 4 cm^{-1} resolution and 16 rates of scans.

MALDI-TOF-MS

Bruker Autoflex Speed MALDI-TOF mass spectrometer with an accelerating voltage of 19 kV was employed with each spectrum scanning 2000 shots. For the sample preparation, α-cyano-4-hydroxy-cinnamic acid matrix was used in acetonitrile (10 mg mL^{-1}), 0.1% TFA. The analyte solution (1 μL, 10 mg mL^{-1}) in acetonitrile mixed in 1 μL of matrix solution, (50 : 50 v/v, CHCA/acetonitrile) and placed in stainless steel sample plate and allowed to dry.

Morphological study of the nanofabric

The compound's internal crystalline bulk morphology was studied using high-resolution transmission electron microscope (HRTEM) supplied by JEM-2100, JEOL at 200 kV. Powder samples were drop cast by preparing a suspension of 0.01 wt% dropped by using a 200 μL microsyringe. The prepared nanofabric was placed in a 300 mesh copper grid in the oven overnight. Images were taken at high resolution and magnification of 5 nm scale, whereas the selected area electron diffraction patterns (SAED) for the samples were captured for determining

Table 1 Preparation parameters applied for the preparation of various composition solutions and electrospinning nanofibre production

Composition	Sample ID	Solution mixing time (h)	Solution mixing temperature (°C)	Flow rate (ml h^{-1})	Working distance (cm)	High voltage (kV)
PLA	P	6	45	1	12	12
15% ZL PLA	PZ15	12	45	1	12	12
25% ZL PLA	PZ25	12	45	1	12	12
1% SNC 15%ZL PLA	$PZ15S_1$	12	45	1	12	12
1% SNC 25%ZL PLA	$PZ25S_2$	12	45	1	12	12

crystalline rings. The average dimensional calculations were done using the Image J® software.

The topography view for powder and the nanofabric mat was obtained using Field Emission Scanning Electron Microscope (FESEM) (Sigma, Zeiss, GmbH, 2–4 kV accelerated voltage) and was treated with conductive gold sputtering unit for 30 s before placing under the equipped microscope. For the powder sample preparation, a suspension (0.01 wt%) was made and sonicated for 10 min, and drop casted over an aluminum foil covered glass slide of 3 × 3 mm dimension. For the nanofabric, the sample was placed over a carbon black tape and both adhered over the stub.

For examining the elemental composition of the prepared nanofabric with mapping, elemental distribution energy dispersive X-ray (EDX) spectroscopy (Oxford Instruments, UK) operated at ~20 kV (SAED) was used. The powdered samples (~2 mg) were floated over the carbon black tape, with gold sputtering for 30 s and placed for analysis.

Thermo-gravimetric analysis (TGA)

The thermal degradation behaviour of the prepared samples were analysed using TGA, supplied by PerkinElmer, TGA4000. Sample weight of ~8–9 mg were taken in an unladen alumina crucible and programmed to heat from 30 to 700 °C at 20 mL min^{-1} of continuous N_2 flow.

Contact angle analysis

For the water race analysis, contact angle measurement was performed using Kruss, DSA-25, Expert model (Germany). (1 × 1) cm (L × B) film form was prepared for the analysis. The instrument settings were set at 27 °C, and water dropping amount at a single time was set as 2 μL distilled water with a drop rate 0.16 mL min^{-1}. Thereby, the water dropping by the syringe over the specimen was captured using a video mode, and measurement was made for different times using Young's Laplace equation.

Contact angle hysteresis

Wettability of the material surface of the masks was measured using contact angle.

$$\cos\theta_\gamma = \left(\frac{\cos\theta_{adv} + \cos\theta_{rec}}{2}\right) \quad \text{(i)}$$

here θ_γ is the Young's contact angle. In the case of an ideal smooth surface, Young's contact angle is considered as an equilibrium contact angle. However, the literature shows that the Young's contact angle could be determined by taking an average of both advancing and receding contact angles.

For those partially wet surfaces, factors affecting are interfacial tensions of solid-vapour, solid–liquid, and liquid–vapour. Therefore, the equilibrium contact angle (θ_e) is the function of these factors.

$$\cos\theta_e = \left(\frac{\gamma_{sv} - \gamma_{sl}}{\gamma_{lv}}\right). \quad \text{(ii)}$$

where, γ_{sv}, γ_{sl} and γ_{lv} are considered as interfacial tensions of solid-vapour, solid–liquid, and liquid–vapour respectively.

$$H = \theta_{adv} - \theta_{rec}$$

$$\theta_{adv} = \theta_\gamma + kH$$

$$\theta_{rec} = \theta_\gamma - (1-k)H \quad \text{(iii)}$$

where, the positive slope of the curve $\theta_{adv} - H$ is k and $0 \le k \le 1$. For such cases in solid–liquid systems, the curves $\theta_{adv} - H$ deviates from linearity at higher values of H.

Mask breathability, porosity, and reusability

The breathability mechanism of these prepared masks was performed by filling the beaker with DI water and covering the beaker mouth with our prepared facemask. Then, silica gel was placed over the fabric and heated till 40 °C. Thus, when silica gel was placed over its surface, there is a change in colour from blue to light pink. One water droplet was also placed on the face-masks surface in order to understand the hydrophobicity of the mask's outer surface. On heating, the membrane is permeable to water vapour. Thus, when silica gel is placed over the membrane, colour changes from blue to light pink.[28]

Air permeability is defined by the airflow *via* a given area of a material influenced by porosity of the material, which in turn impact their openness. Therefore, the following equation can also be correlated based on the calculation

$$\in = \frac{W_{wet} - W_{dry} \times 100}{\rho_{water} \times A \times h} \quad \text{(iv)}$$

where, W_{wet} and W_{dry} represent the wet weights and dried material weights (g); ρ_{water}, water density in g cm^{-1};[3] whereas; A and h indicate the area (cm^2) and thickness (cm), respectively, of the material.

Here, we performed an evaluation for reusability of the fabric prepared using simple ethanol cleaning, a method by dipping. For analysing the reusability of masks, static contact angles of the masks were tested, and its morphological analysis (through FESEM) was done in order to understand the mask morphology by dipping the masks in 75% ethanol for 5–24 h in four cycles.[10]

Antibacterial activity by disc diffusion

The antimicrobial activity of the prepared PLA/ZL fabric layer was determined using the disc diffusion method. Firstly, 100 μL each for bacteria *E. coli and S. Aureus*, comprising a cell content of (10^5 CFU mL^{-1}) was placed on sterile nutrient agar prepared in deionized water according to the standard procedure on Petri dish and spread by a 10 μL inoculation loop. Then, samples of antibiotic (Gentamicin) and prepared fabric were cut in disc shape (0.5 cm in diameter) and then cultured at 37 °C for 24 h. This was followed by optical images and inhibition zone measurement of bacterial cells by measuring the diameters of the inhibition zones of the plates. Indeed, inhibition zone have shown the antibacterial effect of the prepared powder against both *E. coli* and *S. aureus*, (examples of Gram-negative and Gram-positive bacteria) respectively. The effectiveness of

antimicrobial activities can be seen by naked eye by the large diameter of the inhibitory zone.

Bacterial colony count

Bacterial counts for the prepared materials (ZL and SNC) were determined by colony growth count using plate count agar (PCA), (supplied by HIMEDIA) media. 23.5 g DI water solution was prepared in a 250 mL volumetric flask. The solution was properly mixed by sterilizing and autoclaving at 120 °C for 20 min. These were cooled to 45–50 °C and poured into sterile plastic Petri dishes and left for drying. Using 10 μL smooth surface disposable inoculation loops, streaking of the gel surface was done. Then, 10 mg of the prepared powder was dissolved in 1 mL sterile water using a vortex mixer. Each of the samples was diluted to a dilution factor of 10^{-6} in order to get a countable plate. Prepared plate samples were incubated at 35 °C for 72 h. After incubation, each plate was measured by a colony counter.

Virus reduction study

The velogenic NDV strain Bareilly, Baby Hamster Kidney fibroblast cells (BHK-21) was used in this study.[29] ZL coated nanofabric samples with varying concentrations were then incubated with virus dilution (10^{-6}) for 10 min. The extracted viral dilution was added to the seeded BHK-21 cells. The infection was allowed to proceed for 72 h in presence of Dulbecco's modified Eagle's medium (DMEM) supplemented with methyl cellulose and 2% fetal bovine serum (FBS). After 72 h, post treatment was performed with methanol for removing dead cells that were stained with 0.5% crystal blue stain. All the virus reduction studies were performed after post-infection of NDV, and imaging of the sterilized 12-well plate was done by ChemiDoc.

Results and discussion

Structural and morphological analysis

Structure of the oligomer formed was analysed by NMR and FTIR.[30] The structural details of LA and ZL were compared by their peak positions with their shifts, as shown in Fig. 1. As reported, for only oligomers, the peaks of OLLA are obtained at 5.13, 1.56, and 1.24 ppm, which represent –CH protons of OLLA and $-CH_3$ protons and $-CH_3$ protons of hydroxylated OLLA, respectively.[31] The extra new peaks observed at 5.05, near 4.26, 4.09, 1.24, and 1.19 ppm were attributed to the –CH protons of repeating lactyl units, terminal –CH adjacent to Zn^{2+} of repeating unit, terminal –CH protons of hydroxylated lactyl units, $-CH_3$ of lactyl units at terminal groups, and $-CH_3$ protons of hydroxylated lactyl units at terminal groups, respectively. The lactic acid proton NMR shows peaks at 4.02 and 1.06 attributing to terminal –CH and $-CH_3$ protons. The magnified plot (inset: Fig. 1(c)) shows the presence of repeat lactyl units, which confirms the formation of oligomer chains with Zn^{2+} ions, thereby leading to the synthesis of ZL.

Fig. 2(a–c) shows the FTIR spectra of LA, ZL, and PZL25, which were used to study the structural formation and chemical footprints. For lactic acid, the band at 3430 cm^{-1} corresponds to the O–H stretching vibration. Whereas for the case of ZL, there is shifting of the OH group, which signifies the formation of

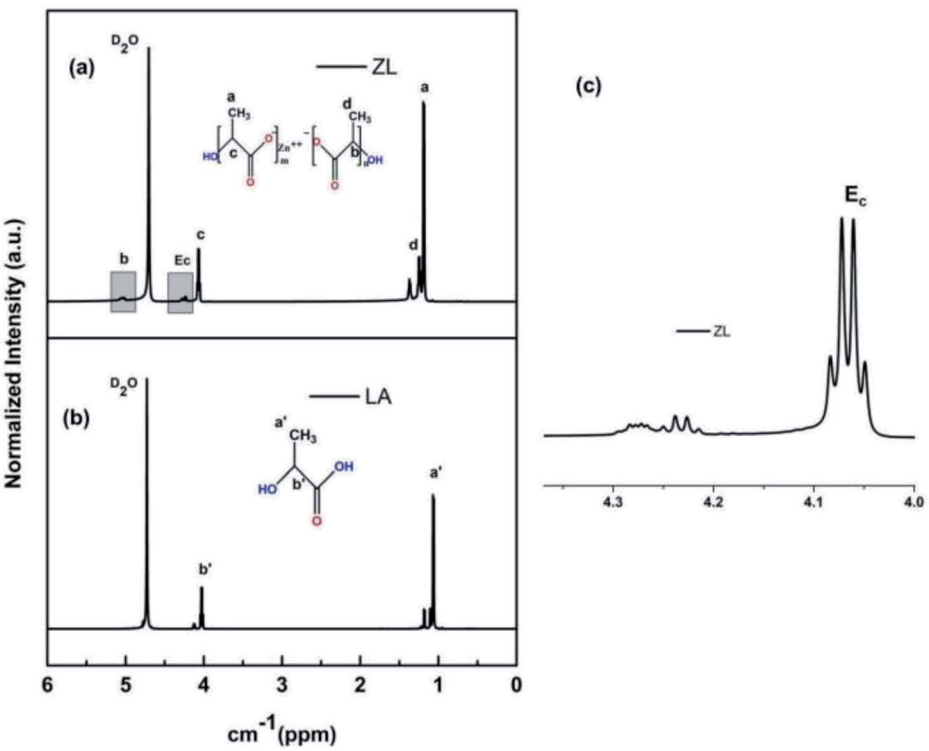

Fig. 1 (a) 1H-NMR spectrum of ZL (b) lactic acid, LA (c) magnified image of ZL spectra within the range of 4–4.3 ppm.

a bond with the –OH group of lactic acid. The –C=O bond stretching vibration at 1745 cm^{-1}, the –C–O– bond at 1379 cm^{-1}, and the asymmetric stretching vibration of the –COO– bond at 1589 cm^{-1} suggest the formation of ZL. The band at 1666 cm^{-1} results from the bending mode of water absorbed by ZL. The strong peak at 1117 cm^{-1} with an intense hump at 1091 cm^{-1} is due to the linkage between Zn and C(O)–O–C stretching vibrations. Demonstration on oligomer synthesized with lactic acid by the appearance of the –C–O–C– bond, characterized by a signal at wavenumber 1174 cm^{-1} was reported.[32] Appearance of a new peak around 460 cm^{-1} is due to the Zn–O linkage that signifies successful preparation of ZL. The spectrum PLAZ25 shows characteristic peaks at 2938, 1380, and 898 cm^{-1} that can be attributed to the stretching vibration of O–H, stretching, deformation, and rocking vibrations of C–H, respectively. The PLAZ25 nanofabric was prepared by solution mixing of ZL and PLA under simple magnetic stirring conditions so no linkage between the ZL and PLA can be seen from the PLAZ25 spectrum. The sharp peaks at their particular positions thereby suggest that the matrix (PLA) is chemically stable even after mixing a higher percentage of ZL.

This analysis was performed for the synthesized ZL sample. The resultant spectra verified the investigation of the species (Zn) taking part in the synthesis of ZL.

$$A = 72x + M_{Zn}(63.5) + M_K{}^{+}(39) + M_{Li}{}^{+}(7) \quad (v)$$

$$B = 72x + M_{Zn}(63.5) + M_{Na}{}^{+}(23) + M_{Li}{}^{+}(7) \quad (vi)$$

The term "x" is the number of lactyl repeat units with M_w value of 72 Da each, M_{Zn} (63.5), $M_{Li}{}^{+}$ (7), $M_{Na}{}^{+}$ (23), and $M_K{}^{+}$ (39) are the molecular weights of zinc powder, lithium ion, sodium ion, and potassium ion, respectively, attached with the PLLA chains.

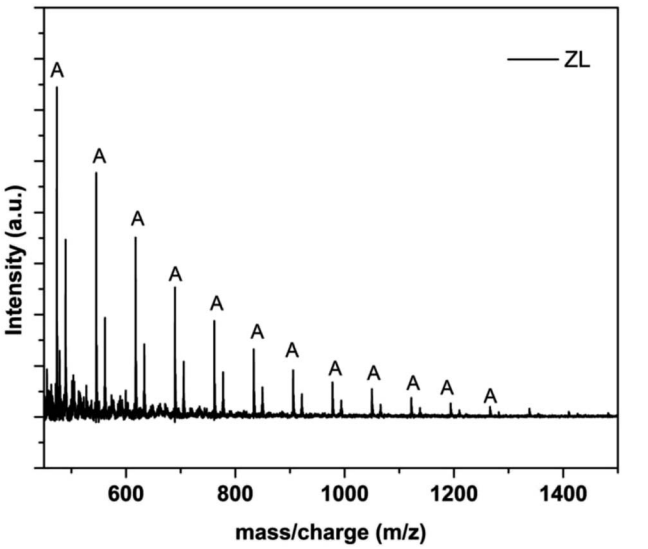

Fig. 3 MALDI-TOF-MS spectrum of ZL synthesized by microwave assisted technique using LiCl, NaCl, and KCl, as cationizing agents with signals separated by 72 units.

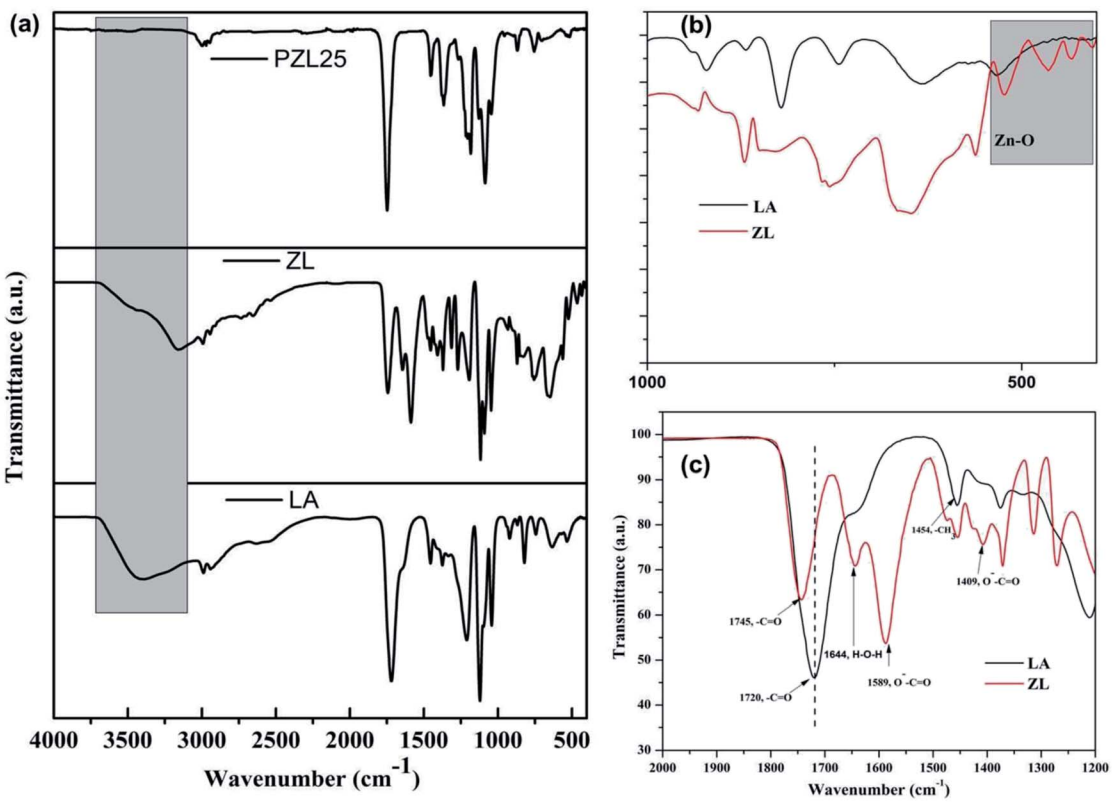

Fig. 2 FTIR spectra of (a) LA, ZL, and PZL25, (b) magnified spectra of LA and ZL (c) spectral range of LA and ZL from 1200–2000 cm^{-1}.

Trans-esterification, may lead to redistribution of chain lengths and formation of polymers with odd numbers of lactyl units separated by a series, 72 units.[33] PLA with neutral C_4H_9O end group and with cationizing agents gives signals with m/z corresponding to n-mer + for corresponding cations (Li^+, Na^+, or K^+). This shows macromolecules are converted into ionic species in this case by intentionally attached cationizing agents. The spectra (Fig. 3) clearly show the intensity of signals denoted as A values from m/z = 473.443 (for 5-mer unit) to m/z = 1266.136 (for 16-mer unit) following the same trend by a difference of 72 units. Therefore, ZL synthesized by zinc contains single trend of chain obtained at masses by equation (v) and hence confirms the presence of terminal ended lactyl chains grafted in zinc surface showed by the schematic diagram (Fig. 1(c)).

Fig. 4(a–d) represents FESEM and X-ray energy dispersive spectroscopy micrographs. It displayed the morphologies of ZL and elemental mapping of the prepared ZL and mat based on electrospinning of $PZ15S_1$ nanofibres in order to have a qualitative determination of the material distribution with PLA. The FESEM micrograph of ZL clearly shows surface roughness due to the presence of short PLA chains. Moreover, the corresponding ZL mapping shows the presence of Zn, C, and O, confirming the formation of ZL from Zn powder. The elemental composition in wt% of Zn is ~33 wt%, which also satisfies the Zn powder amount in (wt%) for the microwave synthesis of ZL *i.e.* ~29%. In

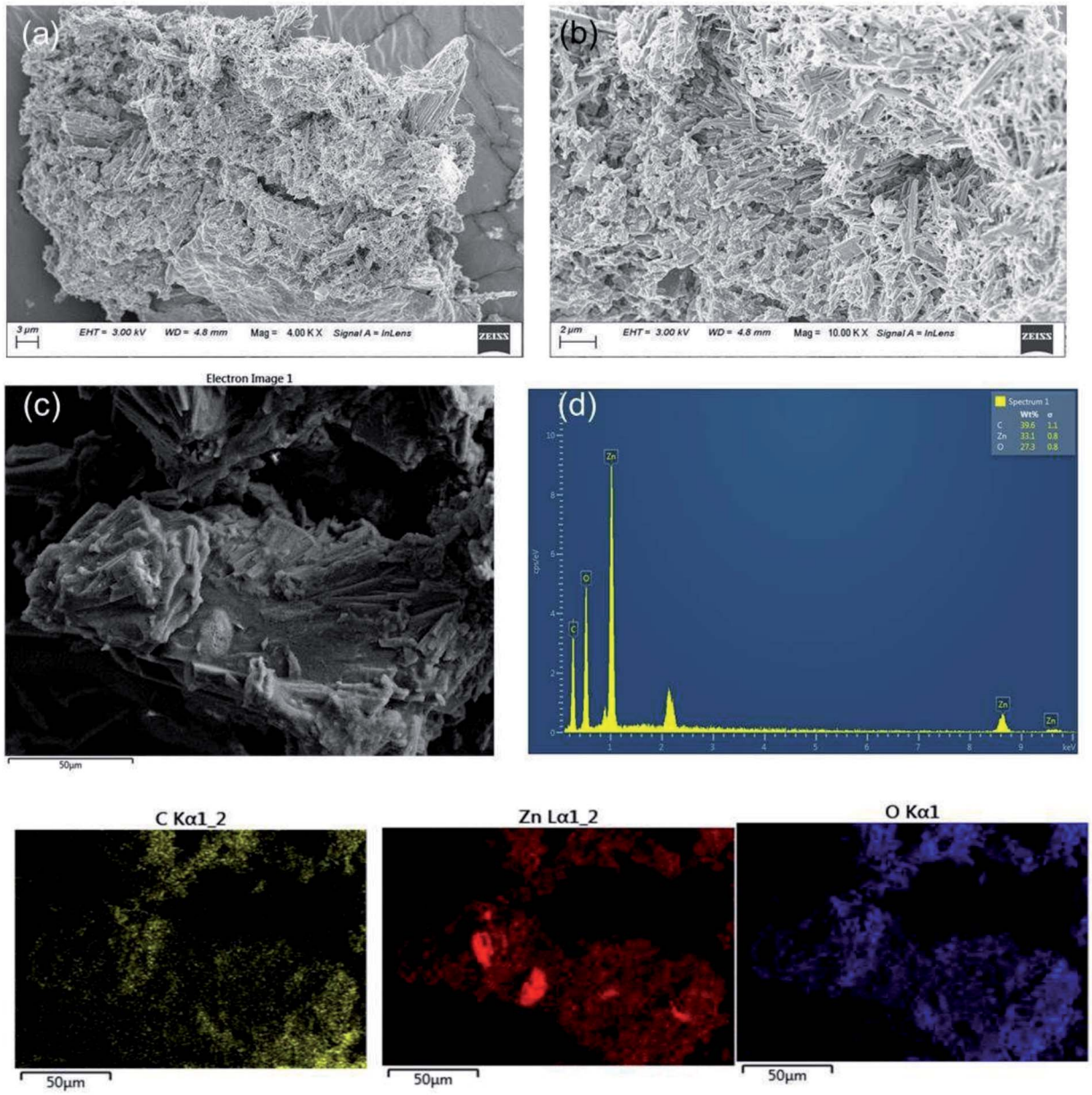

Fig. 4 (a) FESEM image showing zinc lactate powder on a 3 µm scale, (b) magnified image showing ZL surface roughness due to the presence of grafted PLA chains, (c) EDX analysis with its elemental composition (d) mapping for C, Zn, O content with wt% composition.

addition, EDX analysis was also performed to study the elemental composition of electrospun fabrics (concentration of fillers in the nanofabric is at 15% ZL and 1% SNC) as shown in Fig. S1.† Here, Fig. 5(a–f) displays several SEM micrographs associated with the final morphology of PLA and PLA/ZL/SNC nanofabric mat. The average fibre diameters had been calculated using Image J software from the SEM images, and the values were found to be 2.5 ± 2 μm for the PLA nanofibres (Fig. 5(a)), 15% ZL over PLA, for comparison, for a commercially available PP fabric, FESEM image was taken that has average diameter of 17 ± 3 μm as shown in (Fig. 6(b)). Moreover, for the PZ15 nanofibre mat, the fibre diameter decreased to 1.5 ± 2 μm and few with 5.1 ± 2 μm, which suggests uneven formation of nanofibres after incorporation of ZL (Fig. 6(c)). However, when there is an incorporation of SNC with PZ15, there is uniformity in the fibre diameter having average fibre diameter of 1.4 ± 2 μm as shown in (Fig. 5(e and f)).

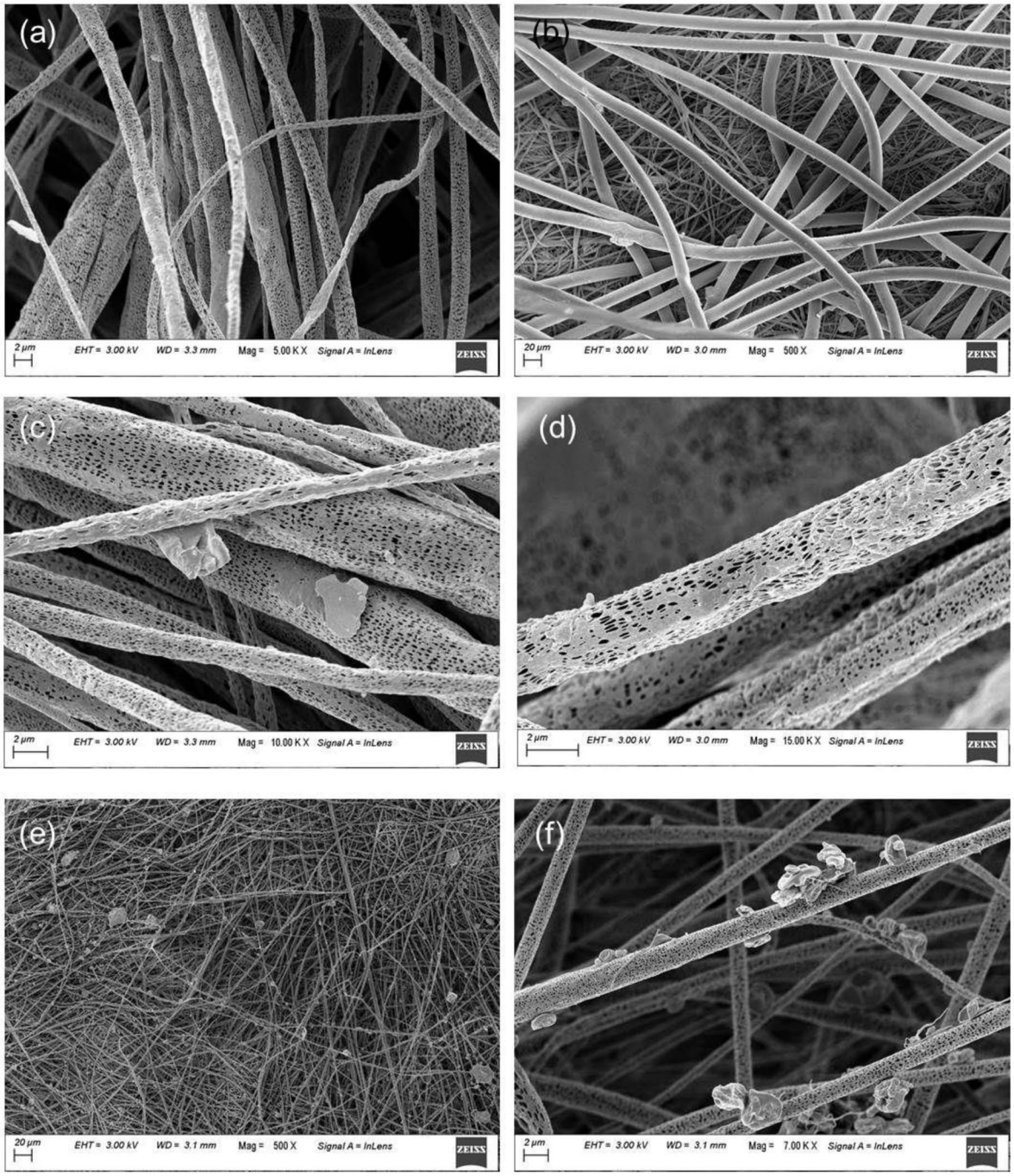

Fig. 5 FESEM micrographs of (a) PLA nanofibers, (b) PZ15 electrospun nanofibers compared with non-woven PP micro fabric, (c) PZ15, (d) magnified surface of PZ15, (e) PZ15S1 nanofiber micrograph showing the distribution of filler (15% ZL and 1% SNC), (f) decorated distribution of ZL and SNC nanoparticles over PLA fibers *via* electrospinning method.

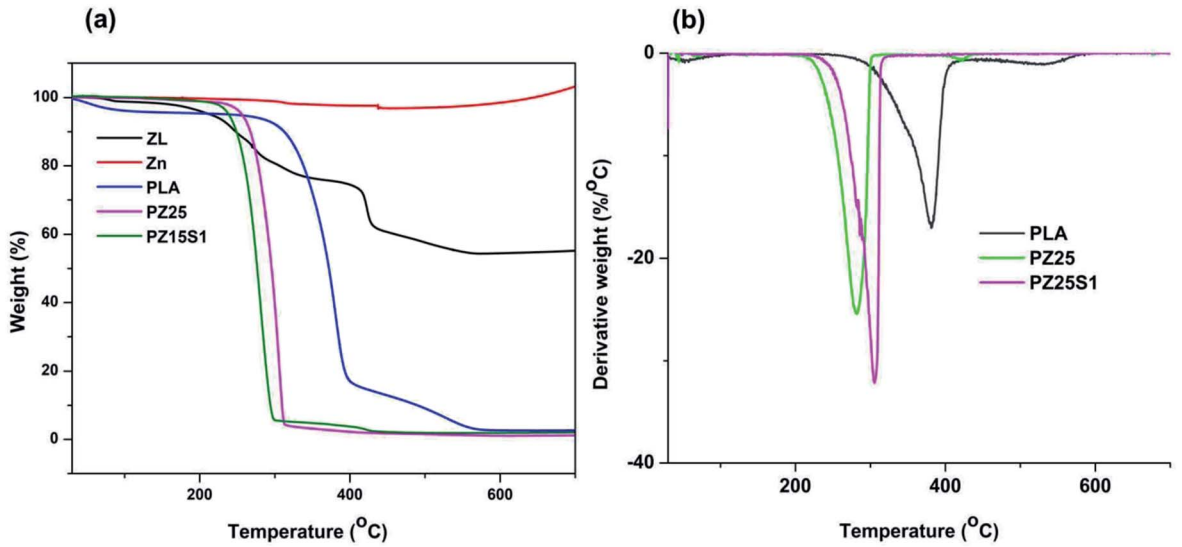

Fig. 6 (a) Thermo-gravimetric analysis of ZL, Zn, PLA, PZ25, PZ15S1 and (b) derivative thermogram (DTG) curve of PLA, PZ25, and PZ15S_1.

Thermal analysis

TGA is an effective method to study the thermal stability and amount of PLA chains grafted with Zn powder. The thermal performance of zinc powder has been studied and found that zinc powder is thermally stable until 438 °C. Subsequently, oxidation of Zn powder takes place, which is obvious from the TGA spectra (Fig. 6(a)) by weight gain.[34] Whereas for the case of ZL, a two-step degradation occurred, where 1st step maximum degradation occurred around 270 °C due to short PLA chains grafted with Zn powder whereas 2nd step maximum degradation occurred at 425 °C because of Zn powder. As Zn is thermally stable until 438 °C for the case of ZL, it can be seen from the carbon residue that the remaining 55% of Zn was un-grafted, thereby maintaining thermal stability up to 700 °C. TGA plot revealed (Fig. 4(a)) that short PLA chains are grafted with Zn powder, as generally PLA degradation starts around 270–400 °C.[35] ZL spectra confirmed that there were around 25% of grafted chains of PLA with Zn powder as PLA chains are thermally stable between 267–400 °C. From the spectra of PLA nanofabric, the onset thermal decomposition temperature is above 270 °C but for the cases of PZ25 there is a decrease of ~44 °C in the onset temperature (T_{onset}). The thermal behaviour is mostly evaluated on the basis of maximum degradation temperature (T_{max}), where the maximum weight loss takes place. From the DTG graph (Fig. 4(b)), it can be seen that there is a decrease in the maximum temperature for PZ25 and PZ15S_1 than PLA due to the presence of short chains of ZL that may start degrading the long PLA chains lowering the temperature. When we consider the DTG spectra for PZ15S_1, T_{max} was found to be 308 °C, which was higher than PZ25 T_{max} *i.e.* 280 °C that was due to the presence of SNC, which had increased the temperature. Furthermore, percentage grafting and percentage conversion of ZL has been calculated by the following eqn (i) and (ii). The results showed ZL percentage grafting and percentage conversion was ~47% and ~150% respectively.

$$\text{Percentage grafting (\%)} = \frac{\text{final weight of ZL} - \text{inial weight of Zn powder}}{\text{initial weight of Zn powder}} \times 100 \quad \text{(vii)}$$

$$\text{Percentage conversion (\%)} = \frac{\text{final weight of ZL}}{\text{initial weight of Zn powder}} \times 100 \quad \text{(viii)}$$

Mask wettability analysis. For nPLA, the static contact angle obtained is 126° ± 3°, which indicates the hydrophobic nature of the nanofabric (Fig. S2†). The hydrophobicity of the nanofabric mat can be attributed to fibre surface and texture. For PZ25, it is 112° ± 3°, less than neat PLA nanofabric, which shows the effect of ZL. A decrease in value on the wettability is due to the presence of short chain ZL incorporated into PLA matrix based masks. But the addition of ZL in PLA did not change surface energy significantly although contact angle reduced from 126° ± 3° to 112° ± 3°, promoting hydrophobicity (Fig. S2†). However, for the modified nanofabric, there is negligible change in WCA, even after 15 min in static conditions. In addition, we found that using SNC in PLA/ZL nanofabric, there was an enhancement in contact angle, which was similar to commercial PP nanofabric used, which is due to the presence of hydrophobic domains in SNC. Therefore, conclusion can be drawn that treatment of PLA nanofabric with 25% ZL and 1% SNC enhanced the hydrophobic nature of the fabric. As an enhancement of the fabric, surface hydrophobicity will also ensure that saliva or sneezing droplets will not easily pass through it.

Mostly, contact angle hysteresis has been raised due to surface roughness and chemical heterogeneity between advancing contact angle and receding contact angle. Therefore, for real surfaces, the advancing θ_{adv} and receding θ_{rec} contact

Table 2 Data representing contact angle hysteresis with surface free energy and slope. Regression represents the linear model efficacy

Sample	C.A. hysteresis	Advancing C.A. (θ_{adv})	Receding C.A. (θ_{rec})	Surface free energy for (θ_{adv}) (mN m^{-1})	Surface free energy for (θ_{rec}) (mN m^{-1})	Slope	Regression
PZ25	10	120.0 ± 1.0	110.4 ± 11.7	11.5	16.8	0.7	0.99
$PZ25S_1$	63	125.6 ± 0.3	61.9 ± 18.7	8.7	46.6	0.7	0.99
$PZ15S_1$	26	115.3 ± 0.6	89.3 ± 6.1	19.8	29.6	0.7	0.99
PLA	51	130.3 ± 0.3	79.5 ± 2.3	6.7	35.7	0.8	0.98
PP	22	117.1 ± 1.0	95.0 ± 8.1	13.5	25.0	0.7	0.98
PZ15	25	113.0 ± 0.7	88.0 ± 4.2	14.7	28.0	0.8	0.96

angles were considered, which plays an important role to obtain the state of wettability. In general, θ_{adv} indicates the maximum contact angle of the solid surface whereas θ_{rec} illustrates the minimum contact angle of the surface. In addition, contact angle hysteresis explains the degree of drop adhesion onto solid surfaces as higher contact angle hysteresis possesses stronger drop adhesion. Fig. S3† shows the receding contact angle and hysteresis calculated for the tested samples. Interestingly, for the nanofabric surface compared to that of pristine PP surface, low contact angle hysteresis was observed that shows lower droplet adhesion, which is desirable in the case of masks for protection from viral as well bacterial and dust particulates.

The linear dynamic modelling for all the test samples has been evaluated to understand the effect of ZL over PLA nanofibres. The θ_{adv} and θ_{rec} values were calculated both experimentally and by a linear model at 27 °C (Fig. S4†). The θ_{adv} and θ_{rec} strongly suggest the applicability of this model for the system PLAZL mask, which might be due to the good porosity maintained on the electrospun nanofabric surface. The slope (k) values for the curves and hysteresis (H) values are shown in Table 2. When ZL and SNC were added, there is no such significant effect on the θ_{adv} and θ_{rec} for fabricated electrospun fabrics as calculated by the Young's contact angle. Nevertheless, it can be observed that the hydrophobic nature of the fabricated nanofabric is significantly determined by surface topography and due to incorporated nature of additives or fillers.

Mask breathability, porosity and reusability. We successfully demonstrated good breathability of the nanofabric over the substrate together with maintaining wettability of the nanofabric surface. Our strategy of electrospinning PLA based fibres and comparison with PP based fabric was successful, which was evident from our (Fig. 7(a and b)) breathability experiment. The silica gel over the nanofabric surface changed its colour from blue to pink signifying its water vapour permeability.

Air permeability or airflow through a material area is influenced by its openness, which affects its porosity. Fig. 8 shows the measured porosity of samples. Interestingly, for the PP fabric, high porosity value was observed *i.e.* 79.2% compared to that for the modified PLA nanofabric (76–46%). The high porous structure in terms of porosity value indicates high air permeability efficiency. The decrease in porosity for the modified fabric can be attributed to the utilization of fillers ZL and SNC that have reduced or mutilated the porous structure. Also, high concentration of ZL and SNC in PLA nanofibres decreases the porosity of the fabric. Although PZ15 and $PZ15S_1$ showed good porosity percentage when compared to PP and can be further optimized and utilized for face mask preparation.

For analysing reusability of the masks static CA for the fabric were tested (Fig. S5†), and its morphological analysis was done in order to understand its morphology dipping the masks in

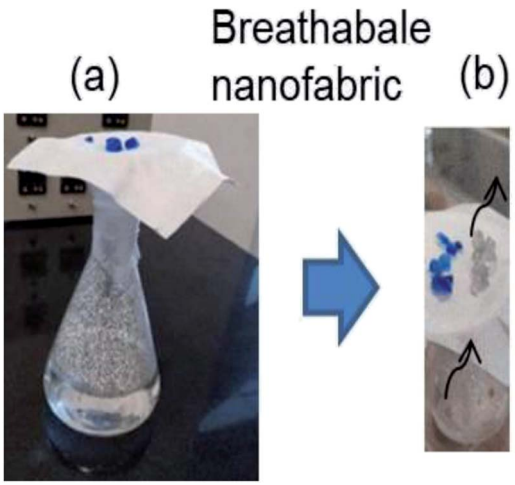

Fig. 7 (a, b) Silica gel placed over nanofabric changed its colour from blue to pink.

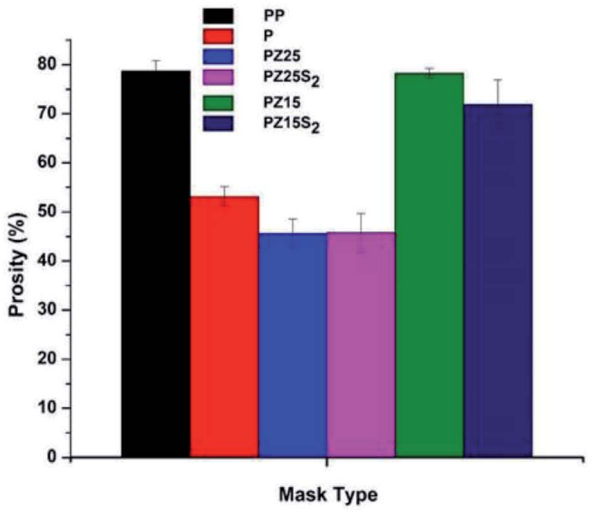

Fig. 8 Porosity percentage of prepared facemasks in order to understand its air permeability.

Table 3 Comparative data for reusability test of facemasks dipped in ethanol solution from 5min to 24 h in four different cycles

Sample	1st R (5 min)	2nd R (30 min)	3rd R (12 hours)	4th R (24 hours)
PZ25	125 ± 5	120 ± 7	120 ± 4	116 ± 2
PZ25S1	125 ± 4	123 ± 2	119 ± 3	119 ± 2
PZ15S1	129 ± 8	125 ± 3	125 ± 5	123 ± 4
PLA	124 ± 3	122 ± 4	122 ± 3	118 ± 6
PP	132 ± 2	125 ± 3	118 ± 3	112 ± 9
PZ15	112 ± 4	123 ± 2	123 ± 5	108 ± 4

75% ethanol for 5 min to 24 h in four cycles. After dipping treatment from SEM analysis, it was clear that the modified PP mat did not undergo any significant morphological changes. This test confirmed our prepared modified PP fabrics have good indicator in terms of reusability, consumer end-use, and commerciality (Table 3). From Fig. S6,† no significant decrease in hydrophobicity for the samples even after 4th cycle of reuse was seen. This parameter signifies that our prepared compostable fabric can be reused up to 4 times without compromising its surface properties like hydrophobicity and surface texture and can be used as facemasks. After 4th cycle, FESEM images showed negligible surface changes for the prepared fabric as shown Fig. 9(a–c). Similar characterization technique was used elsewhere[10] where they demonstrated reusability of the facemasks up to 10 times after ethanol dipping. Here, we also proved its reusability using the mentioned analysis without any morphological changes, which is considered as a performance parameter of the prepared facemasks.

Antibacterial activity of ZL incorporated into PLA nanofabric

Firstly, antibacterial activity has been studied by the disc diffusion assay and then by bacterial growth count. Fig. 10 shows the nutrient agar plate cultured with *E. coli*, *S.aureus* treated with antibiotic (control), and the prepared PLA/ZL fabric. Repetitive analysis was performed for the fabricated nanofabric layers. It was found that significant bactericidal activities against microorganisms can be seen when compared with antibiotic (10 mcg) after 24 h of incubation. Overall, the results indicate killing of bacteria by clearly visible inhibition zones, which was due to the release of Zn^{2+} ions that damages the cell membrane and penetrates the intracellular contents. Compared to *S. aureus*, nanofabric showed a larger inhibition zone toward *E. coli* of around 1 cm, which is depicted using blue lined circles with arrow head.

The concentration of ZL was changed (10–200 μg mL^{-1}). It was found that 200 μg mL^{-1} concentration give significant effective bactericidal activities against microorganisms. Whereas the reported value for ZnO nanomaterial bacterial inhibition concentration is 500 μg mL^{-1} for *E. coli*.[36] ZL may act

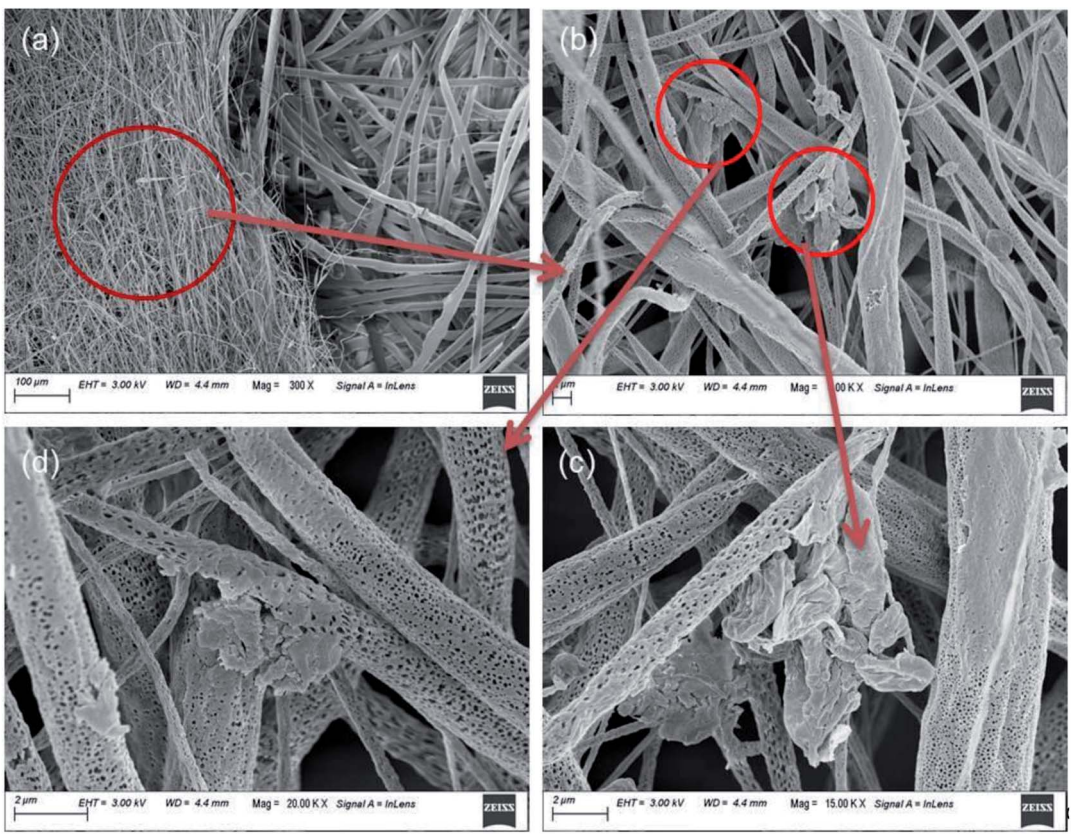

Fig. 9 (a) SEM images of PZ15fabric over commercial PP substrate (for comparing fibre diameter) after 24 h of dipping in ethanol, (b) Distribution of ZL and SNC in the fabric, (c, d) magnified image of distributed ZL and SNC.

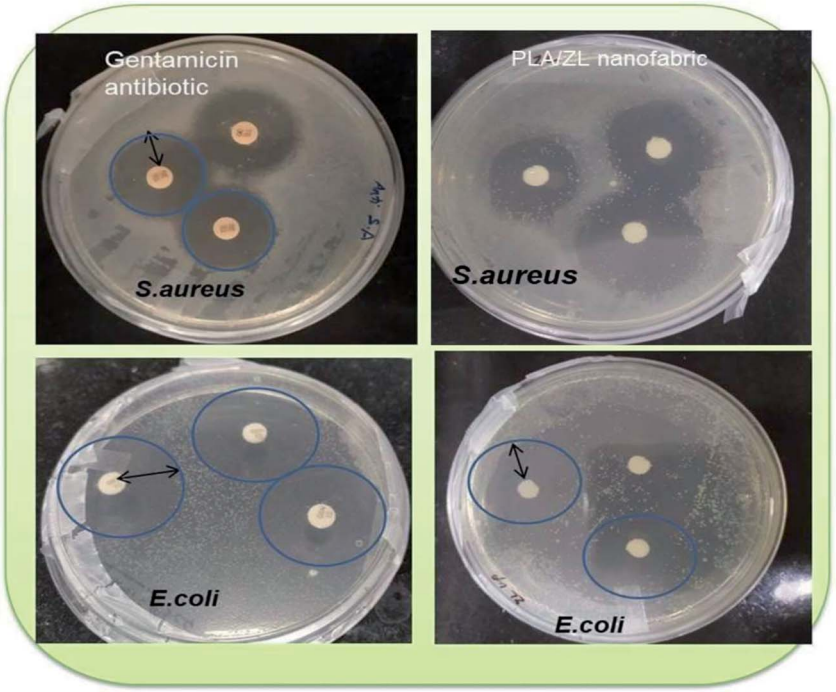

Fig. 10 Visual images (smartphone camera) of inhibition zone by ZL showing similar trend of antibacterial activity against the taken bacteria as antibiotic Gentamicin.

as a better material having superior antibacterial activity against both the Gram-negative and Gram-positive bacteria. This has been proved using viable bacteria counts by dilution method for ZL and SNC against E.coli bacteria and compared with control (no zinc or SNC added only *E. coli*). After 72 h of incubation, visual studies showed zinc significantly reduced the viability of *E. coli* compared to silk nanocrystal and controls shown in Fig. S7.† The reviewed studies have agreed that antibacterial effectiveness of zinc was mostly concentration-dependent and increases with an increase in the concentration of zinc.[37,38]

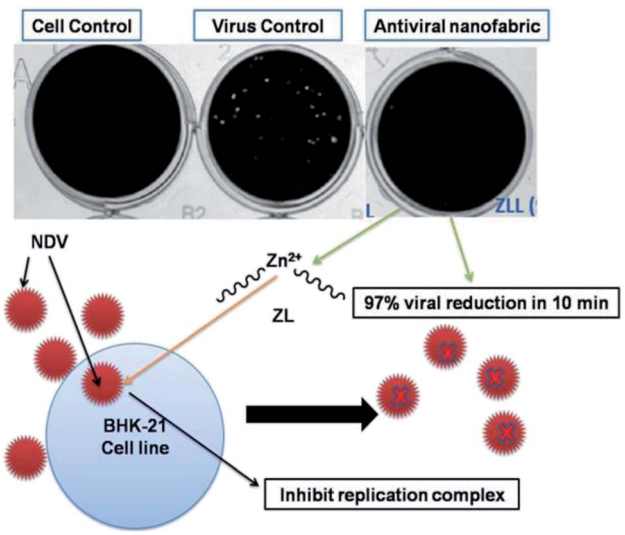

Fig. 11 Schematic antiviral mechanism of the fabricated nanofabric showcasing 97% viral reduction in 10 min of time.

Antiviral analysis

The diluted PP/PLA-ZL nanofabric was tested and observed, and there is significant reduction in plague for the coated nanofabric in 10 min of time, which is 97%. This revealed the antiviral potential against NDV by the inhibition of virus growth. Though at the beginning cell death occurred, but later, this has been resolved after dilution. The mechanism lies in the presence of the taken concentration of Zn^{2+} ion grafted L-lactate oligomer chains, which can engulf the virus by inhibiting its growth as shown in Fig. 11. When compared with the reported studies, we found that the antiviral efficacy here is more than that already reported for prepared facemasks where CuS was used in 3-layered nylon masks (99.9% antiviral efficacy was found in 1 h).[39] Brief description with data for this work has been mentioned elsewhere in the filed Indian patent application (202131013654) which cannot be disclosed in its present form.

Conclusion

In summary, a hydrophobic, antimicrobial, and antiviral nanofabric layer having antiviral efficacy of 97% in 10 min was fabricated comprising of PLA, ZL, and SNC. This antiviral layer was developed from polycondensation reaction of Zn with LA, forming ZL and PLA followed by electrospinning into a non-woven nanofabric for property enhancement. The prepared nanofabric had good breathability and promoted

hydrophobicity, which are the most essential properties of a material for its application as face mask. The prepared SNC based PLA/ZL nanofabric exhibited water contact angle (125.69 $\pm$ 0.35°) even higher than the commercial PP fabric (117.7 $\pm$ 1°). This also indicated that the use of ZL in PLA had no inverse effect on hydrophobicity. Reusability data of the prepared nanofabric demonstrated that it can withstand up to 4 cycles by ethanol dipping/washing treatment without undergoing significant changes in its surface morphology. This clearly suggests that the prepared nanofabric as a mask can be reused several times by treating it with ethanol. The prepared layer further exhibited excellent antibacterial properties against *E. coli* and *S. aureus* in presence of ZL. This novel facial mask preparation technique contributed towards sustainability, biodegradability, and reusability. The functionalized PLA based nanofabric can be used as a protective layer directly or in conventional PP based masks. As future works, multiple layers using hybrid materials with PLA can be studied in detail, focussing mainly on material processing and compostability without compromising its antiviral properties. The current limitation of the work, which can fuel future research interests would be to carry out further research on the solubility problem of ZL and SNC in PLA matrix above 25% and 1%, respectively.

Author contributions

DH: conceptualization; data curation; formal analysis; investigation; methodology; software; validation; visualization; roles/writing – original draft; writing – review & editing, NKK: formal analysis; investigation, writing – review & editing, AK: supervision, VK: conceptualization; funding acquisition; project administration; resources; supervision; validation; visualization; writing – review & editing.

Conflicts of interest

There are no conflicts to declare.

Acknowledgements

The authors sincerely thanks Department of Science and Technology (DST) Govt. Of India, for the necessary grants (project number: xENVSPNxDST00860xxVK014) provided for smooth running of the current research work. The authors acknowledge the Centre of Excellence for Sustainable Polymers (CoE-SusPol) funded by the Department of Chemicals and Petrochemicals (DCPC); Central Instruments Facility (CIF), Viral Immunology Laboratory, Department of Biosciences and Bioengineering, at Indian Institute of Technology Guwahati (IIT Guwahati) for all the research facilities.

References

1 G. Gorrasi, A. Sorrentino and E. Lichtfouse, *Environ. Chem. Lett.*, 2020, 1–4.
2 A. V. Mueller, M. J. Eden, J. M. Oakes, C. Bellini and L. A. Fernandez, *Matter*, 2020, **3**, 950–962.
3 O. O. Fadare and E. D. Okoffo, *Sci. Total Environ.*, 2020, **737**, 140279.
4 O. Das, R. E. Neisiany, A. J. Capezza, M. S. Hedenqvist, M. Försth, Q. Xu, L. Jiang, D. Ji and S. Ramakrishna, *Sci. Total Environ.*, 2020, **736**, 139611.
5 Y. Zhao, R. Chen, R. Ni, H. Liu, J. Li and C. Huang, *J. Text. Inst.*, 2020, **111**, 1231–1237.
6 M. Ali and Q. T. Aina, *Environmental Contaminants Reviews*, 2020, **3**(1), 32–36.
7 X. Huang, T. Jiao, Q. Liu, L. Zhang, J. Zhou, B. Li and Q. Peng, *Sci. China Mater.*, 2019, **62**, 423–436.
8 K. P. Chellamani, D. Veerasubramanian and R. S. Vignesh Balaji, *J. Acad. Ind. Res.*, 2013, **2**, 320.
9 S. Jiang, Y. Chen, G. Duan, C. Mei, A. Greiner and S. Agarwal, *Polym. Chem.*, 2018, **9**, 2685–2720.
10 S. Ullah, A. Ullah, J. Lee, Y. Jeong, M. Hashmi, C. Zhu, K. Il Joo, H. J. Cha and I. S. Kim, *ACS Appl. Nano Mater.*, 2020, **3**, 7231–7241.
11 Y. Turovskiy and M. L. Chikindas, *Probiotics Antimicrob. Proteins*, 2011, **3**, 144–149.
12 S. A. Read, S. Obeid, C. Ahlenstiel and G. Ahlenstiel, *Adv. Nutr.*, 2019, **10**(4), 696–710.
13 D. N. Marreiro, K. J. C. Cruz, A. R. S. Oliveira, J. B. S. Morais, B. J. S. A. Freitas, S. R. S. Melo, L. R. Santos, B. E. P. Cardoso and T. M. S. Dias, *Br. J. Nutr.*, 2021, 1–21.
14 A. V. Skalny, L. Rink, O. P. Ajsuvakova, M. Aschner, V. A. Gritsenko, S. I. Alekseenko, A. A. Svistunov and D. Petrakis, *Int. J. Mol. Med.*, 2020, **46**(1), 17–26.
15 C. P. Singh, R. L. Vaishna, A. Kakkar, K. P. Arunkumar and J. Nagaraju, *Cell. Microbiol.*, 2014, **16**, 1354–1365.
16 A. F. Parlin, S. M. Stratton, T. M. Culley and P. A. Guerra, *PLoS One*, 2020, **15**, 1–19.
17 R. Patwa, N. Soundararajan, N. Mulchandani, S. M. Bhasney, M. Shah, S. Kumar, A. Kumar and V. Katiyar, *Biopolymers*, 2018, **109**(11), e23231.
18 J. Xue, T. Wu, Y. Dai and Y. Xia, *Chem. Rev.*, 2019, **119**, 5298–5415.
19 D. S. Zhang, X. Y. Liu, J. L. Li, H. Y. Xu, H. Lin and Y. Y. Chen, *Langmuir*, 2013, **29**, 11498–11505.
20 N. K. Kalita, S. M. Bhasney, A. Kalamdhad and V. Katiyar, *J. Environ. Manage.*, 2020, **261**, 110211.
21 M. Murariu and P. Dubois, *Adv. Drug Delivery Rev.*, 2016, **107**, 17–46.
22 A. Z. Naser, I. Deiab and B. M. Darras, *RSC Adv.*, 2021, **11**(28), 17151–17196.
23 A. F. Alwan, *IOP Conf. Ser.: Mater. Sci. Eng.*, 2019, **571**(1), 012085.
24 N. Tripathi and V. Katiyar, *J. Appl. Polym. Sci.*, 2016, **133**(21), 43458.
25 H. T. Au, L. N. Pham, T. Ha, T. Vu and J. S. Park, *Macromol. Res.*, 2012, **20**(1), 51–58.
26 S. Feng, F. Zhang, S. Ahmed and Y. Liu, *Coatings*, 2019, **9**(8), 525.
27 E. Buluş, G. S. Buluş and F. Yakuphanoğlu, *J. Mater. Electron. devices*, 2020, **4**, 21–26.
28 A. Baji, K. Agarwal and S. V. Oopath, *Polymers*, 2020, **12**(2), 492.

29 K. Shokeen, A. Srivathsan and S. Kumar, *Virus Res.*, 2021, **292**, 198223.
30 A. V. Raghu, G. S. Gadaginamath and T. M. Aminabhavi, *J. Appl. Polym. Sci.*, 2005, **98**(5), 2236–2244.
31 A. K. Pal and V. Katiyar, *J. Polym. Res.*, 2017, **24**(10), 1–21.
32 F. G. Orozco, A. Valadez-González, J. A. Domínguez-Maldonado, F. Zuluaga, L. E. Figueroa-Oyosa and L. M. Alzate-Gaviria, *Int. J. Polym. Sci.*, 2014, 365310.
33 M. Florczak, A. Michalski, A. Kacprzak, M. Brzeziński, T. Biedroń, A. Pajak, P. Kubisa and T. Biela, *React. Funct. Polym.*, 2016, **104**, 71–77.
34 L. Qi, X. Weng, L. Yuan, B. Wei, X. Wu, G. Huang, X. Du and H. Liu, *Infrared Phys. Technol.*, 2020, **110**, 103458.
35 A. K. Pal and V. Katiyar, *Biomacromolecules*, 2016, **17**, 2603–2618.
36 M. Li, L. Zhu and D. Lin, *Environ. Sci. Technol.*, 2011, **45**, 1977–1983.
37 M. M. Almoudi, A. S. Hussein, M. I. Abu Hassan and N. Mohamad Zain, *Saudi Dent. J.*, 2018, **30**, 283–291.
38 K. Kannan, D. Radhika, A. S. Nesaraj, K. K. Sadasivuni, K. R. Reddy, D. Kasai and A. V. Raghu, *Mater. Sci. Energy Technol.*, 2020, **3**, 853–861.
39 C. Hewawaduge, A. Senevirathne, V. Jawalagatti, J. W. Kim and J. H. Lee, *Environ. Res.*, 2021, **196**, 110947.